# Structural evolution and competing magnetic orders in polycrystalline GdN films

Kartik Senapati,* Thomas Fix, Mary E. Vickers, Mark G. Blamire, and Zoe H. Barber
*Department of Materials Science and Metallurgy University of Cambridge, Cambridge CB2 3QZ, United Kingdom*
(Received 14 October 2010; revised manuscript received 18 November 2010; published 10 January 2011)

We report a study of the structure and magnetic behavior of polycrystalline GdN films grown at room temperature by reactive magnetron sputtering. By controlling the relative fraction of reactive species during film growth, we observe a continuous crossover from soft ferromagnetic films into relatively hard ferromagnetic films. While samples with a Curie temperature ($T_c$) of less than ~60 K showed low coercive fields, a significant increase in the hysteretic loss was observed for samples with $T_c \gtrsim 60$ K. Accompanying the change in the magnetic behavior of the films, signatures of a secondary phase of GdN (GdN-II) were observed in x-ray diffraction measurements. Such dual-phase samples (with GdN and GdN-II) showed an exchange bias effect, which confirmed that the GdN-II phase was antiferromagnetic. The Curie temperatures of the dual-phase samples were found to be much higher than the reported value of $T_c$ for GdN. We believe that the origin of the antiferromagnetic phase and the enhanced $T_c$ of ferromagnetic GdN can be closely related to nitrogen vacancies in the samples. While the local strain induced by nitrogen vacancies can strengthen antiferromagnetic ordering in GdN-II, the change in carrier concentration due to the nitrogen vacancies strengthens the ferromagnetic ordering in the GdN phase. Hall effect measurements showed that transport properties of polycrystalline GdN films can be tuned from almost-insulating to semimetallic behavior by varying the amount of nitrogen in the samples. Amid a continuing debate on the origin of ferromagnetism in GdN, our data show considerable support for a carrier-mediated mechanism of ferromagnetism.

DOI: 10.1103/PhysRevB.83.014403 PACS number(s): 75.70.Ak, 75.30.Et, 75.60.Ej

## I. INTRODUCTION

Gadolinium nitride (GdN) is one of the most intriguing and widely studied members of the rare-earth monopnictide group of compounds.[1–20] While electronic transport in GdN has been reported to exhibit semimetallic,[6] semiconducting,[2] and insulating[8] behavior, the magnetic ordering has also remained a debatable issue.[3,6,12,15,16] GdN shows ferromagnetic ordering below ~60 K,[10–15] with a saturation magnetization of 7 $\mu_B$/Gd, similar to the magnetic properties of the better-known ferromagnetic semiconductor EuO.[21] However, the origin of magnetic ordering in these compounds is believed to be entirely different.[12,15] Ferromagnetism in EuO results from a nearest-neighbor *f-f* interaction via an on-site *f-d* exchange mechanism.[12] The on-site *f-d* exchange effectively leads to a mixing of the f and d orbitals, parametrized by ($t_{df}$ $\Delta_{df}$), where $t_{df}$ is the *d-f* hopping integral and $\Delta_{df}$ is the minimum energy difference between the *d* and the f bands.[12] Unlike EuO, the 4*f* band in GdN lies well below the Fermi level;[11,12,22] that is, $\Delta_{df}$ is large. As a result, the *f-d* mixing parameter in GdN is too weak to induce nearest-neighbor *f-f* interaction and a $T_c$ close to EuO. Therefore a carrier-mediated, Ruderman-Kittel-Kasuya-Yoshida (RKKY)-type[23] nearest-neighbor interaction,[5,9,17,19] enforced by the on-site *f-d* exchange mechanism, is considered the most likely candidate for ferromagnetic ordering in GdN.

Recent calculations by Duan *et al.*[13] have suggested that a next-nearest-neighbor antiferromagnetic superexchange mechanism coexists in these compounds along with the RKKY-type nearest-neighbor interaction. Recently, Mitra *et al.*[17] have suggested that, in addition to the 4*f* moments ($7\mu_B$), a small 5*d* moment appears on the Gd site of the GdN lattice due to the *f-d* exchange. This extra moment is compensated by an opposite moment induced on the surrounding N sites, effectively ordering the Gd-5*d* and *N-p* orbitals antiferromagnetically. Since the the Gd-*f* orbitals are locked to the Gd-*d* orbitals via the *f-d* exchange, the nearest-neighbor Gd-*f* moments are forced to order ferromagnetically. This model, however, predicted a maximum $T_c$ of ~10 K. In very recent work[19] a modified RKKY model for GdN predicted a $T_c$ of ~60 K for a carrier concentration of $\sim 8 \times 10^{19}/\text{cm}^3$. The authors suggested that the intrinsic $T_c$ of GdN may indeed be low, as calculated by Mitra *et al.*, while the experimentally observed values of $T_c$ (between 60 and 80 K) may be due to additional carrier doping of the conduction band from various degrees of impurities and vacancies in the films. However, for a carrier concentration of $\sim 8 \times 10^{20}/\text{cm}^3$ (similar to the value obtained by Ludbrook *et al.*[18]), this model predicts no FM transition down to 0 K. The current understanding of the bulk magnetic order in GdN appears to suggest a sensitive balance between AFM and FM orders, prone to extraneous effects such as strain and N vacancies. Similar uncertainties exist in the electronic transport behavior of GdN, with band structure calculations placing it in between semimetals and semiconductors.[15] A wide range of experimental data and theoretical approaches toward the understanding of the intricately connected electronic and magnetic ordering in rare-earth monopnictides has been reviewed by Duan *et al.*[15]

The revived interest in GdN is primarily motivated by its prospective application as a spin-filtering material for low-temperature spintronics applications. For integration into spin-active devices, ambient-temperature growth of GdN is particularly useful to avoid thermal interdiffusion in magnetic heterostructures during the growth process. Therefore, process optimization and understanding of the magnetic interactions in polycrystalline films grown at ambient temperatures are a timely necessity. In this context we have studied the evolution of magnetization behavior of polycrystalline GdN thin films deposited using varied relative fractions of component species (Gd and N) during film growth. A strong dependence of the

 

physical properties on the nitrogen partial pressure ($p_{N_2}$) and sputtering power was observed, similar to other transition metal nitrides.[24] Films with Curie temperatures ranging from 20 K to 140 K were obtained. The saturation magnetization of our samples was found to be lower than the ideal Hund's rule value of $7\mu_B$/Gd ion. In a previous publication[20] we focused on a series of GdN samples prepared at a fixed value of $p_{N_2}$ and varying sputtering power. A significant increase in coercive field ($H_c$) was observed at higher sputtering powers (corresponding to an increase in the supply of Gd). X-ray diffraction measurements showed the existence of a second phase of GdN (GdN-II) with a slightly larger lattice parameter. The estimated relative volume fraction ($f$) of the GdN-II phase using the relation $f = 1 - (M_s/M_{s(\mathrm{Max})})$, where $M_{s(\mathrm{Max})}$ is the maximum saturation moment obtained in a series of samples grown at fixed $p_{N_2}$, was found to follow the change in coercive field, confirming that the magnetic interaction between GdN and GdN-II is the source of enhanced coercivity. An exchange bias effect was observed[20] in the samples containing both GdN and GdN-II phases, which indicated that GdN-II is antiferromagnetic in nature. The Nèel temperature was found to be ~36 K.

In the present paper we report a detailed study of the magnetization behavior of GdN films prepared under various $p_{N_2}$ and sputtering powers. Changes in magnetic properties have been analyzed in terms of changes in the structural parameters of GdN and GdN-II. Finally, the issues of the origin of the antiferromagnetic phase and the enhanced $T_c$ in ferromagnetic GdN are discussed in relation to nitrogen vacancies in the samples.

## II. SAMPLE PREPARATION AND MEASUREMENTS

GdN films were deposited on $5 \times 5$ mm$^2$ single-crystal Si substrates with a 250-nm thermally grown $SiO_2$ layer by reactive dc magnetron sputtering, using a high-purity Gd metal (99.9%) target. The base pressure of the UHV sputtering chamber was $\sim 2 \times 10^{-7}$ Pa, before introducing a mixture of high-purity Ar and nitrogen gases. The background oxygen and $H_2O$ levels, monitored via a residual gas analyzer, were minimized by a prolonged Ti-sublimation pumping cycle. This is a vital step of the deposition, which reduces the oxygen contamination in the GdN films, known to suppress the $T_c$.[1] Prior to the deposition of GdN, a 50-nm layer of NbN was deposited to avoid formation of $GdSi_2$ at the film/substrate interface. We find that GdN films grown directly on the $Si/SiO_2$ substrate react rapidly and flake off the substrate within a few days. A 50-nm capping layer of NbN was deposited on the GdN layer (between 50 and 75 nm thick) to isolate it from atmospheric moisture. Due to the intentional, nonoptimal deposition conditions of NbN, the superconducting transition temperatures of the buffer and the capping NbN layers were less than 5 K in all cases. Therefore, the magnetization measurements, performed at temperatures $\gtrsim$10 K, were not affected considerably by the NbN layers. Films were sputtered under a pressure of 1.5 Pa at a target-substrate distance of 3.4 cm. The sputtered flux was directed onto a rotating substrate stage through a small gap in a shield, placed in front of the target. This arrangement allows subnanometer-level control of thickness and provides an effective thermal shield against unwanted substrate heating by the plasma.

In the sputtering environment the Gd:N ratio was varied by changing the $N_2$ partial pressure in the sputtering gas and, also, by varying the target power density (a higher power leads to an increase in Gd flux). Due to the large mass difference between Gd and nitrogen ions, the kinetic energy of these two reactive species may differ considerably in the sputtering environment, and compound formation may occur at the target surface and/or between target and substrate. This leads to a complex relation between Gd:N ratio and GdN formation. Four series of samples were prepared, using 4%, 6%, 8%, and 10% nitrogen partial pressures. At each fixed value of $p_{N_2}$, the sputtering power was varied from 0.49 to 0.96 W/cm$^2$ in steps of ~0.067 W/cm$^2$. The deposition time was adjusted to maintain a constant thickness of the GdN films at a fixed $p_{N_2}$.

Magnetization measurements were performed in a vibrating sample magnetometer based on a variable temperature insert. Isothermal hysteresis loops were measured up to a maximum field of 5 T, applied along the plane of the films. A small paramagnetic contribution from the buffer and capping layers of NbN was subtracted from the measured values of magnetic moment, along with a diamagnetic contribution from the substrate and the sample holder. The temperature stability during the isothermal measurements was better than 0.05 K. Temperature-dependent, zero-field-cooled (ZFC) and field-cooled (FC) magnetization curves were measured with a 500-G field while warming the samples at the moderate rate of 2 K/min.

## III. RESULTS

### A. Magnetic response

In Fig. 1 we compare the general trend of magnetic hysteresis measured at 10 K for samples grown at varying $p_{N_2}$. Clearly, there is a significant increase in the coercive field ($H_c$) in the high-power-grown films, particularly at lower $N_2$ partial pressures. The magnetization of high coercivity samples did

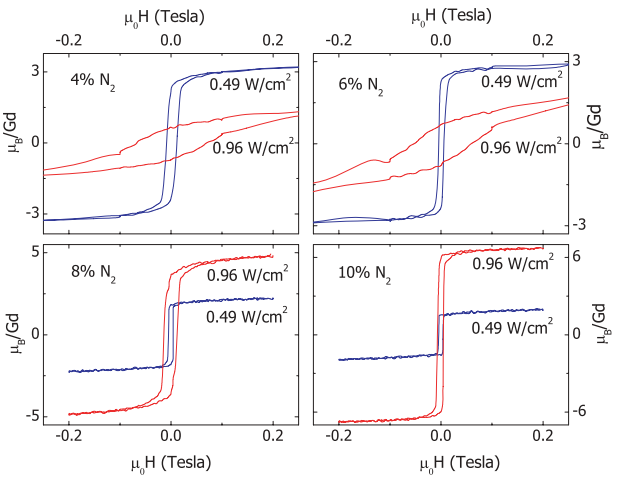


FIG. 1. (Color online) Isothermal magnetization loops of GdN films deposited under varied $N_2$ partial pressures, measured at 10 K. For each $p_{N_2}$ pressure, hysteresis loops are shown for the lowest and the highest sputtering powers used for deposition.

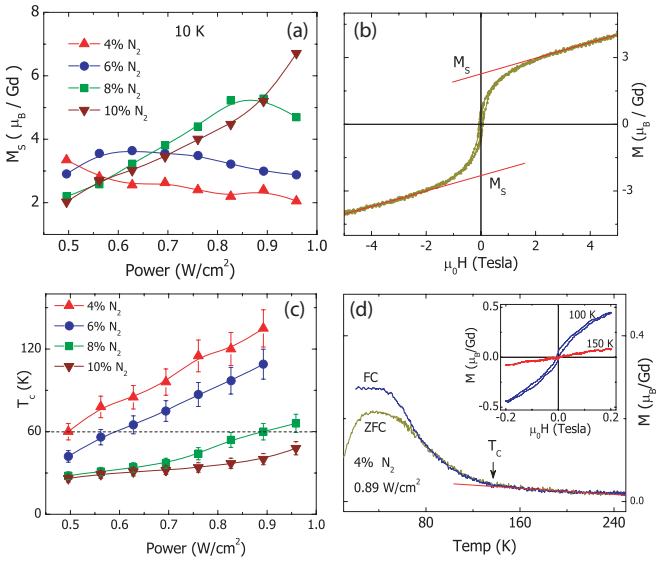


FIG. 2. (Color online) (a) Saturation magnetization measured at 10 K plotted as a function of sputtering power. (b) A representative high-field hysteresis loop, showing the convention used to calculate the saturation magnetization $M_s$. (c) Variation of the $T_c$ of GdN films with sputtering power. (d) Representative ZFC and FC magnetization curves, showing the convention used to determine $T_c$. Inset: magnetization loops of the same sample above (150 K) and below (100 K) the $T_c$.

not saturate up to a field of 5 T. Saturation magnetization of the samples was obtained from high-field magnetization loops by extrapolating the high-field linear region to 0 field, as shown in Fig. 2(b). In most cases the saturation magnetization ($M_s$) was significantly less than the theoretical value of $7\mu_B$/Gd. However, films with $M_s$ close to $7\mu_B$/Gd were obtained at high powers in high $p_{N_2}$. Figure 2(a) shows the sputtering power dependence of $M_s$ at fixed $p_{N_2}$. This plot suggests that $M_s$ varies nonmonotonically with sputtering power, with a maximum value that shifts to higher powers for higher $p_{N_2}$. In general, samples in the region of decreasing $M_s$, after the peak value, showed relatively higher $H_c$, irrespective of $p_{N_2}$.

The Curie temperatures of the GdN films as a function of sputtering power are plotted in Fig. 2(c) for various values of $N_2$ partial pressures. $T_c$ was taken as the point of deviation from the high-temperature paramagnetic response, as shown in Fig. 2(d). This method of determining $T_c$ is rather crude and may introduce systematic errors up to 10 K. However, we point out that our discussion concerns the variation of $T_c$ as a funcion of sputtering parameters. Therefore, inaccuracies in determining $T_c$ do not affect the overall discussion. In our GdN films, at all $p_{N_2}$, $T_c$ increased monotonically with increasing power. The dotted line in Fig. 2(c) corresponds to the most widely accepted value of $Tc$ for GdN (60 K).[12,14] Samples with $T_c$ higher than ∼60 K showed considerable coercivity enhancement. Comparing Figs. 2(a) and 2(c) we note that the maximum value of $M_s$, for any specific value of $p_{N_2}$, is achieved for samples with $T_c$ close to 60 K. Since the variation in sputtering power and $N_2$ pressure effectively varies the Gd:N ratio in the sputtering plasma, the observed correspondence between maximum $M_s$ and theoretical $T_c$ may be correlated with a stoichiometric effect.

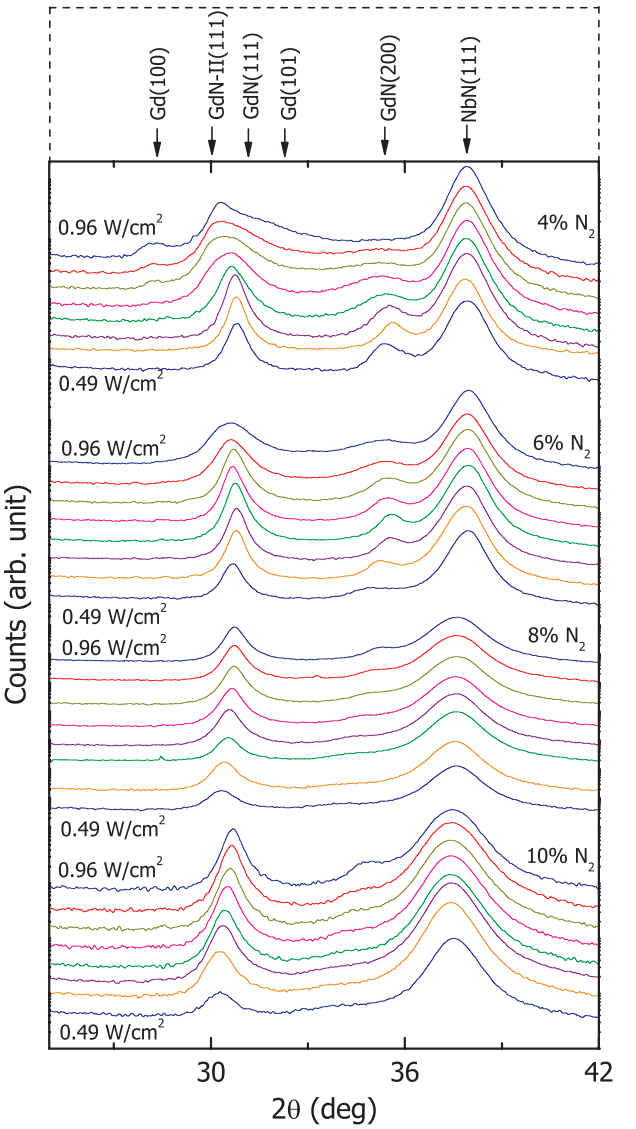


FIG. 3. (Color online) $2\theta$-$\theta$ x-ray diffraction patterns of GdN films grown under various $N_2$ pressures at powers of 0.49, 0.56, 0.63, 0.69, 0.76, 0.83, 0.89, and 0.96 W/cm$^2$. Approximate positions of GdN, GdN-II, Gd, and NbN peaks are shown by the arrows in the top panel.

### B. Structural changes

Further insight can be obtained by studying the structural evolution of the films as a function of sputtering power and $N_2$ pressure. Figure 3 shows the $2\theta$-$\theta$ x-ray diffraction patterns of GdN films grown at various sputtering powers and $N_2$ pressures. The data show polycrystalline face-centered cubic GdN films with the strongest reflections from (111) planes. In the 4% $N_2$–grown samples, note the continuous gradual broadening of the GdN (111) and (200) peaks as the power increases. A closer look at the (111) peaks reveals that this gradual broadening is accompanied by an increasing asymmetry of the peak, indicating the condensation of a secondary phase of GdN (denoted GdN-II) closely associated with the primary GdN phase. No such phase separation (or peak asymmetry) was apparent in the 8% and 10% $N_2$ samples. In these samples, the GdN (111) and (200) peaks

monotonically shifted to higher angles with increasing power. In the series of 6% $N_2$ samples an interesting crossover was observed. Initially, with increasing power (up to 0.63 W/cm$^2$) the GdN peaks shifted to higher angles (similar to 8% and 10% $N_2$ samples), followed by the development of a peak asymmetry and broadening (similar to the 4% $N_2$ samples). This crossover is more discernible in the (200) peaks in this series of samples. Here we draw the attention of the reader to Fig. 2(c), where the Curie temperature of the samples is plotted as a function of sputtering power. Comparing the x-ray diffraction data and the $T_c$ of the 6% $N_2$ samples, it is clear that the structural crossover is closely associated with a magnetic crossover across a $T_c$ of ~60 K. In general, samples with $T_c >$ 60 K show signatures of the GdN-II phase, the fraction of which increases with increasing $T_c$.

## IV. DISCUSSION

Since the condensation of GdN-II phase significantly modifies the magnetic behavior of the films ($T_c$ and $H_c$), it is reasonable to assume that GdN-II is magnetically different from the soft ferromagnetic phase of GdN. Although in Fig. 3 (4% $N_2$) we do observe a small Gd condensation at the highest powers, the enhanced coercivity effect appears long before that.[20] A small amount of Gd nanogranules may only add a superparamagnetic contribution (with extremely low coercivity[25]) to the hysteresis loop. Therefore we can assign the deviations in the magnetic response of GdN films, from the ideal soft ferromagnetic behavior, to the magnetic coupling between GdN and GdN-II phases. Both hard ferromagnetic behavior and antiferromagnetic behavior are likely candidates for the magnetic nature of GdN-II, since both are known to enhance coercivity when coupled to a soft ferromagnet.[26–30] However, FM-AFM systems can be distinguished from soft-hard FM systems by the presence of an exchange bias effect, which is characterized by an offset of the hysteresis loops along the field axis by $H_{Ex}$, the magnitude of exchange bias. Indeed such an exchange bias effect was observed in our GdN films (reported elsewhere[20]) with higher coercivity. Therefore, we conclude that the GdN-II phase is antiferromagnetic. The Nèel temperature of GdN-II (~36 K) was extracted[20] by fitting Malozemoff's random field model[31] for exchange-biased FM-AFM systems to the temperature dependence of $H_{Ex}$.

The exchange bias effect explains the apparent magnetic hardening observed in the GdN films. However, the origin of the antiferromagnetic phase in the samples and an explanation of the enhanced $T_c$ (beyond 60 K) demands a closer look at the correlation between structural and magnetic changes in these films. Since there is clear evidence of the existence of two phases (GdN and GdN-II) in the high-coercivity samples, we have used a professional profile fitting program (Philips ProFit) to deconvolute the individual peaks of GdN and GdN-II. The integral area of the deconvoluted peaks may be used as a rough estimate of the volume fraction of GdN and GdN-II phases in the samples. We mention here that only those samples that showed a measurable exchange bias at 10 K were fitted for separate GdN and GdN-II peaks. Other samples were fitted only for the GdN phase. The diffraction profiles of samples showing signatures of Gd [(100) peak close to $2\theta \sim 28^\circ$ and an enhanced background close to $2\theta \sim 32^\circ$, corresponding to the (101) peak of Gd] were also fitted with hexagonal Gd peaks along with GdN and GdN-II peaks. Since the apparent position of the peaks changes continuously with sputtering power, the final peak positions obtained from each profile fitting were used as initial fitting parameters for the next profile. For example, in the series of 4% $N_2$ samples, the profile fitting of the first (0.49 W/cm$^2$) sample was initialized by manually introducing a GdN-II peak close to the GdN peak. The final parameters obtained from this fit were then used as the initial parameters for the profile fitting of the next sample (0.56 W/cm$^2$), which, in turn, provided the initial parameters for the next sample (0.63 W/cm$^2$). This process was continued up to the sample deposited at maximum power (0.96 W/cm$^2$). Figure 4 shows a sample fitted profile (0.83 W/cm$^2$ and 4% $N_2$) with deconvoluted GdN, GdN-II and Gd peaks. We note that manual introduction of the GdN-II peak into the fitting algorithm, in the first fitted profile, involved an error of ~0.2% in the peak position and up to 20% error in the integral area of the peaks. These errors were estimated by averaging over several fittings of a single profile with slightly different initial parameters. The positions of the peaks were used to calculate the lattice parameters of GdN and GdN-II phases.

In Fig. 5(a) we have plotted the sample saturation magnetization and the lattice parameters of the GdN and GdN-II phases as a function of the Curie temperature, eliminating the dependence on deposition parameters. Similarly, Fig. 5(b) plots the measured exchange bias as a function of $T_c$. Figure 5(c) plots an estimated volume fraction GdN-II:GdN, calculated using the integral area of the respective (111) peaks from the fitted x-ray profiles. The theoretical x-ray scattering intensities of the GdN and GdN-II phases are expected to be similar, because the structure factor is dominated by the Gd

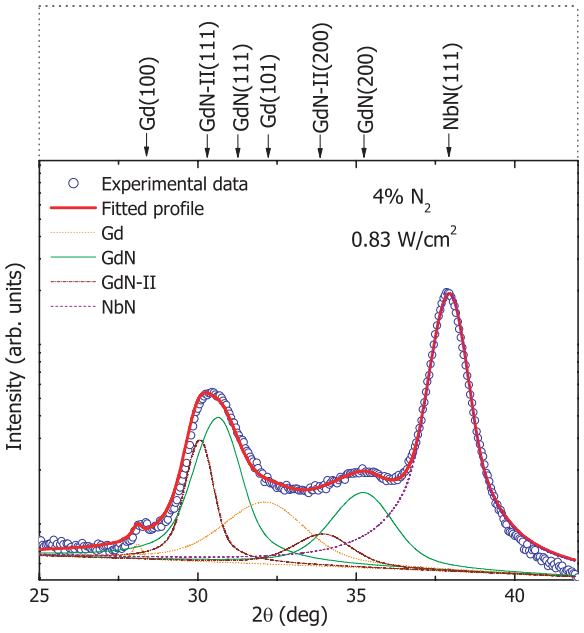


FIG. 4. (Color online) Sample profile fitting of the x-ray data using Philips ProFit. The solid line is the total calculated profile, while dotted and dashed lines are the deconvoluted peaks corresponding to GdN, GdN-II, Gd, and NbN.

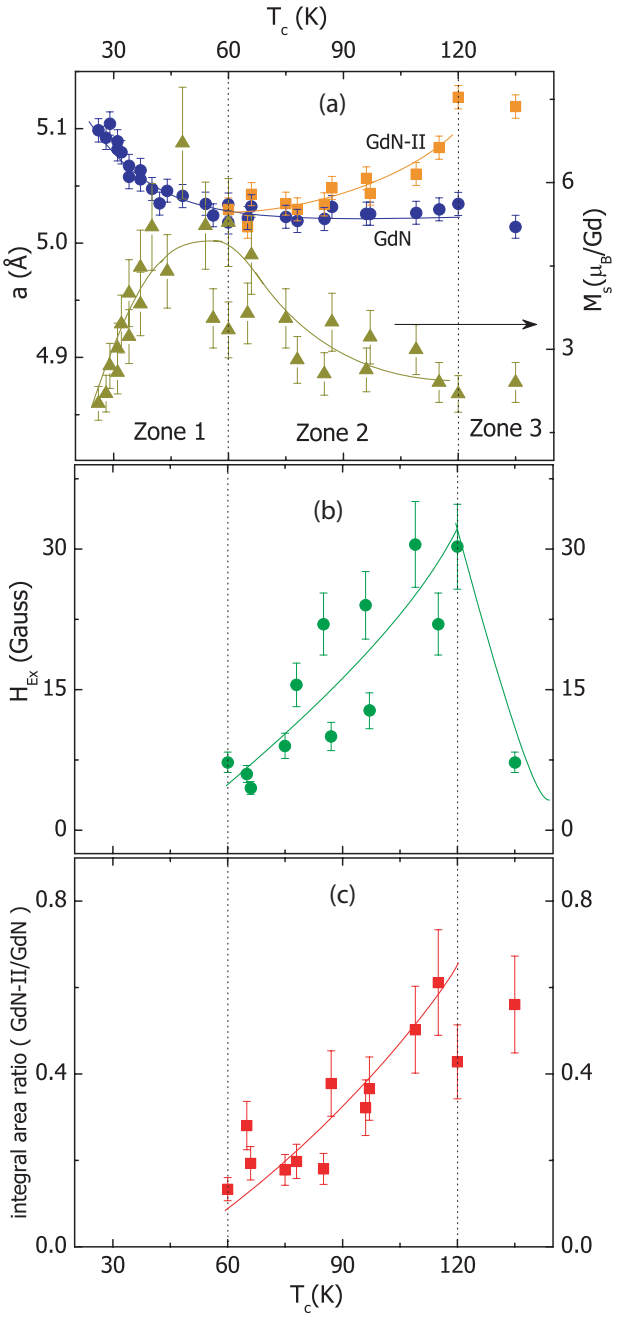


FIG. 5. (Color online) (a) Phase diagram showing the correlation among the Curie temperature $T_c$, the saturation moment $M_s$ (filled triangles), and the lattice parameters ($a$) of the GdN (filled circles) and GdN-II (filled squares) phases. (b) A similar phase diagram plotting $T_c$ and exchange bias $H_{Ex}$. (c) Ratio of (111) peak area GdN-II:GdN obtained from profile fitting plotted as a function of $T_c$. Solid lines in all cases are only to guide the eye.

sublattice. Therefore, in principle, the ratio of the integral areas of the strongest peaks should give a reasonably good estimate of the volume fraction. However, we note that the shared phase boundaries between GdN and GdN-II phases in the homogeneous film may contribute to the scattering intensities of GdN and GdN-II phases in a nontrivial manner. Therefore, in Fig. 5(c) we can only rely on the trend of the volume fraction as a function of $T_c$. The exact values of the GdN-II:GdN ratio, however, do not affect our discussion. Three zones can be readily recognized in Fig. 5, separated by the dotted vertical lines.

*Zone 1*: Increasing $T_c$ accompanies increasing $M_s$ and decreasing lattice parameter of GdN. All data points in this zone belong to either low-power or high-$N_2$pressure samples. Considering the dynamic process of formation of GdN during reactive growth, samples grown with a relatively higher $p_{N_2}$ or low power (low Gd flux) can be either (1) nitrogen rich, with significant N interstitials in the GdN lattice, or (2) Gd deficient, with the packing fraction of the Gd sublattice lower than that of the N sublattice. However, one would expect an increase in lattice parameter with increasing nitrogen interstitials. Here we refer back to the x-ray data of 10% $p_{N_2}$ (Fig. 3). Samples grown with progressively increasing power at a fixed $p_{N_2}$ can be expected to have a decreasing amount of N interstitials due to increased Gd flux and faster deposition rate. Therefore, the lattice parameter should decrease (i.e., GdN peaks should move to a higher angle) with increasing power, consistent with the $p_{N_2} = 10\%$ data in Fig. 3. Therefore, we consider zone 1 to be a nitrogen-rich zone with significant nitrogen interestitials in the GdN lattice. No significant exchange bias was observed in this zone.

*Zone 2*: In this zone, increasing $T_c$ corresponds to decreasing $M_s$. Although the lattice parameter of GdN remains constant in this zone, a significant fraction of GdN-II appears to coexist with GdN. This zone is also characterized by a significant exchange bias as shown in Fig. 5(b). The integral area ratio GdN-II:GdN of the (111) peak, plotted in Fig. 5(c), shows that the strength of exchange bias is directly proportional to the amount of GdN-II in the films. The data in this zone belong to the samples deposited at a relatively higher power or lower $p_{N_2}$. Preliminary x-ray photoemission spectroscopy data confirm a substoichiometric $N_2$ concentration in the samples in this zone (44.5 at % of nitrogen was detected in a sample with $T_c \sim 75$ K, deposited at 0.69 W/cm$^2$ and 6% $N_2$). Based on the deposition conditions of the samples in this zone, they can be argued to be either Gd rich (additional Gd in the interstitials) or N deficient (low packing fraction of the N sublattice). However, we note that most samples in this zone belong to $p_{N_2} = 4\%$ and 6%, which show a decrease in the saturation moment with increasing power [see Fig. 2(a)]. If increasing power leads to an increase in Gd interstitials, then we would expect the opposite trend of $M_s$. Therefore we consider the region $T_c > 60$ K to be a N-deficient zone, with the density of N vacancies increasing with increasing $T_c$. The magnetic behavior of GdN in this zone is controlled by N vacancies.

*Zone 3*: In this zone, although the $T_c$ increases further, the exchange bias drops drastically, to close to 0. In addition, the x-ray diffraction data for these samples show a significant amount of Gd. Therefore it is reasonable to assume that the dominant magnetic interactions in this zone are those of Gd metal. The presence of this Gd-rich zone, as a continuation of the N-deficient zone, further justifies our assumption that the density of nitrogen vacancies is increasing in the samples as the $T_c$ increases in zone 2.

In zone 1 (Gd:N ratio $< 1$) of the phase diagram, one would expect a saturation magnetization less than the theoretical value of $M_s$ for GdN due to the low packing fraction of

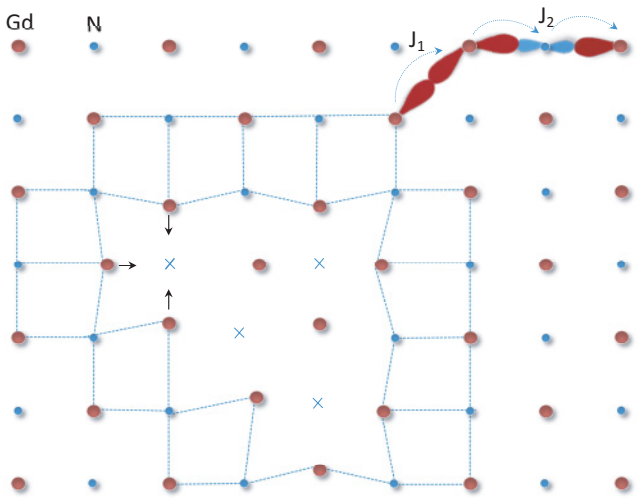


FIG. 6. (Color online) Cartoon depicting the local lattice distortion caused by nitrogen vacancies in a two-dimensional face-centered-cubic lattice, effectively separating the GdN-II phase (dashed lines) from the GdN matrix. $J_1$ and $J_2$ are the nearest-neighbor and the next-nearest-neighbor magnetic exchange interactions.

Gd atoms. As the Gd:N ratio approaches unity, $M_s$ and $T_c$ approach the bulk values of $7\mu_B$/Gd and 60 K, respectively. As the Gd:N ratio exceeds unity, nitrogen vacancies appear in the GdN lattice. In a simplistic picture, as shown in the sketch in Fig. 6, a nitrogen vacancy may lead to a local distortion of the lattice, effectively stretching the unit cells surrounding itself (shown by the dotted lines in Fig. 6). Such local static displacements of transition metals around N vacancies (shown by straight arrows in Fig. 6) have been reported earlier.[32] For example, ion channeling experiments on NbN films have shown an average static displacement of ~0.14 Å of Nb atoms toward the N vacancy.[32] In the presence of a positive lattice strain in GdN, the nearest-neighbor ferromagnetic exchange ($J_1$) between the Gd sites has been shown[13] to decrease. In addition, Duan *et al.*[13] have suggested that the Gd-*X*-Gd ($X$ = P, As, Sb, Bi) superexchange interaction ($J_2^{\text{super}}$) for Gd monopnictides can be expressed by the empirical relation $J_2^{\text{super}} = -n_d(t_{pd}^4/\Delta^3)$, where $n_d$ is the $d$ moment induced by intra-atomic 5*f*-4*d* exchange, $t_{pd}$ is the hopping integral between the N-*p* and Gd-*d* orbitals, and $\Delta$ is the energy difference between the $d$ and the $p$ orbitals of Gd and N, respectively. This interaction $J_2^{\text{super}}$ is antiferromagnetic and of a magnitude similar to that of the total magnetic exchange between next-nearest-neighbor Gd sites $J_2$.[15] In general, all members of the GdX family with a lattice parameter larger than GdN are antiferromagnetic. In GdN the value of $J_2$ decreases considerably[13,15] with increasing lattice parameter, signifying a strengthening of the AFM order. Our result (exchange bias effect only in the nitrogen-deficient zone 2) suggests that the local distortion caused by the nitrogen vacancy is the most likely origin of the antiferromagnetic phase in our films. This idea is further supported by our observation that increasing nitrogen vacancies [going from left to right of the nitrogen-deficient zone in Fig. 5(c)] increases the volume fraction of the GdN-II phase, and consequently, the exchange bias increases [Fig. 5(b)]. In this framework, the increasing trend of exchange bias can only be sustained until the volume fraction of FM and AFM becomes equal. Beyond this critical point, further accumulation of nitrogen vacancies results in a considerable separation of Gd phases from the GdN-II phase, effectively reducing the volume fraction of the AFM phase in the sample. Consequently one would expect a drop in the magnitude of the exchange bias, as shown in Fig. 5(b).

In addition to a local lattice deformation, nitrogen vacancies also add carriers to the conduction band.[18] The effects of additional charge carriers on the physical properties of the ferromagnetic semiconductor EuO have been analyzed by Mauger and Godart.[33] Accounting for the spin polarization of free carriers due to the internal field associated with localized spin polarization, and the small width of the $5d_{t_{2g}}$ band (i.e., low carrier density), they predict[33] a deviation of the magnetization curve from the mean field Brillouin function.[34,35] The most distinguishing features of these electron-doped ferromagnetic semiconductors is the significantly extended ferromagnetic transition region, unlike the sharp transitions in undoped samples following the Brillouin function.[34,35] All our samples in the $N_2$-deficient region show such an extended ferromagnetic transition region. A representative temperature-dependent magnetization curve of a sample with $T_c \sim 85$ K is shown in Fig. 7. Calculated Brillouin functions using the measured saturation moment ($2.55\mu_B$/Gd for this sample) and the ideal Hund's rule value of $7\mu_B$/Gd are superimposed on the experimental data in Fig. 7. We find the closest agreement of the data with the calculated Brillouin function for $S = 2.55$ and $T_c \sim 70$ K. However, the data in Fig. 7 show that magnetic ordering in this sample appears above the mean field value of 70 K. Exact calculations of the temperature-dependent magnetization curves using the Mauger model[33] require knowledge of the on-site *d*-*f* exchange integral and the width of the $5d_{t_{2g}}$ band. Both these parameters are difficult to determine accurately. However, the general concept of the model still applies. Therefore, the apparent enhancement of Curie temperature in zone 2 in Fig. 5 is

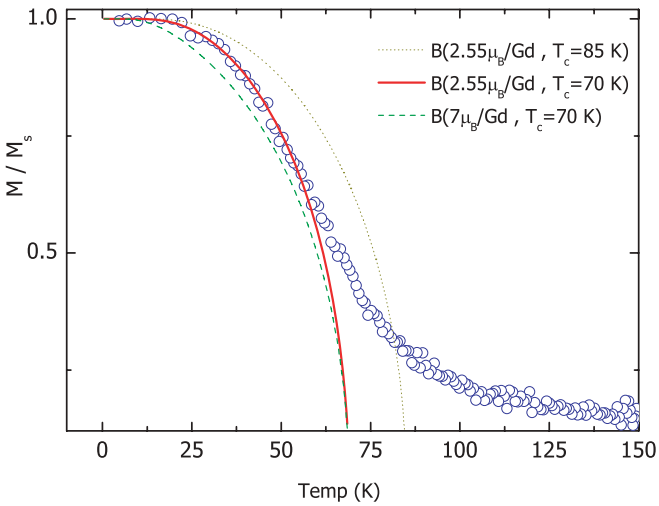


FIG. 7. (Color online) Temperature-dependent magnetization of a GdN film with $T_c \sim 85$ K. Solid and dotted lines are calculated Brillouin functions with $S = 2.55/2$ and $T_c = 70$ and 85 K, respectively. The dashed line is the calculated Brillouin function with $T_c = 70$ K and local spin $S = 7/2$, the Hund's rule value for GdN.

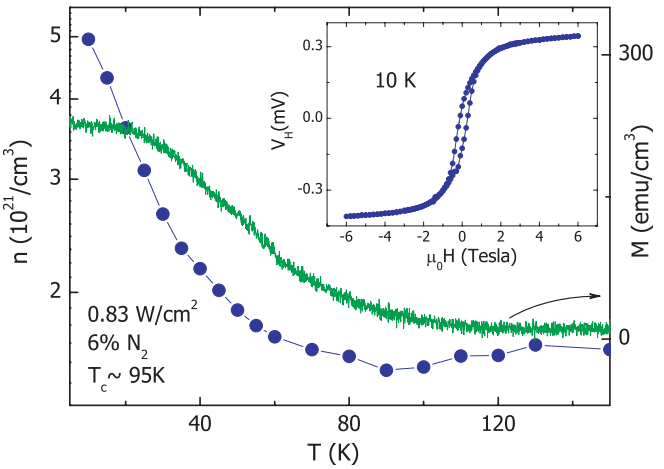


FIG. 8. (Color online) Temperature dependence of carrier concentration obtained from ordinary Hall effect measurements (filled circles) and the temperature-dependent magnetization curve. Inset: measured Hall voltage at 10 K.

suggestive of an additional carrier-induced mechanism in GdN, due to the N vacancies. Similar enhancements in the Curie temperature in EuO, following the Mauger model,[33] have been reported by several authors.[36–38] This was achieved by electron doping of the conduction band via oxygen vacancies[38] or substitution of $Eu^{2+}$ ions by $Gd^{3+}$ and $La^{3+}$.[36,37] Growth dislocations have also been reported to enhance the $T_c$, for example, in EuS.[39]

It is believed that the nearest-neighbor ferromagnetic exchange $J_1$ in GdN is primarily a carrier-mediated coupling of $f$ orbitals.[13,15,17,19] Although the carrier-mediated mechanism is not viable for magnetic exchange in ideally stoichiometric GdN, nitrogen-deficient GdN, due to the enhanced carrier concentration, is ideally suited for this type of interaction. To establish the correlation between carrier concentration and $T_c$, we determined the carrier concentration of several GdN films by Hall effect measurements. For these measurements, 150-$\mu$m-wide tracks were patterned by optical lithography and argon ion milling of ~90-nm-thick GdN films, protected by insulating AlN layers on top and bottom. As shown in the inset in Fig. 8, a large anomalous Hall effect, proportional to the sample magnetization, was observed below $T_c$. Therefore the carrier concentration ($n$) was calculated from the high-field (between 4- and 6-T) slope, which is predominantly due to the ordinary Hall component of the measured Hall voltage. Our preliminary measurements showed a decrease in carrier concentration of almost an order of magnitude in a film with $T_c \sim 40$ K ($n \sim 3.5 \times 10^{20}$/cm$^3$), compared to the carrier concentration in a sample with $T_c \sim 95$ K ($n \sim 1.6 \times 10^{21}$/cm$^3$) at 120 K. In Fig. 8 we show the temperature dependence of carrier concentration for a sample with $T_c \sim 95$ K (deposited at 0.83 W/cm$^2$ and $p_{N_2} = 6\%$). The sharp increase in the carrier concentration below $T_c$ is due to the exchange splitting of the conduction band edge populating the majority carrier band, consistent with earlier experiments on EuO[40] and GdN.[18] The carrier concentration obtained by Ludbrook *et al.*[18] in epitaxial pulsed-laser-grown GdN films ($T_c \sim 70$ K) was ~$3.7 \times 10^{20}$/cm$^3$ at 120 K. The observed correlation between $n$ and $T_c$ in our films strongly supports a carrier-mediated mechanism of ferromagnetism, both the N-rich and the N-deficient zones. Referring back to the N-rich zone in Fig. 5(a), we note that the lattice parameter of GdN decreases simultaneously with an increase in Gd fraction. Both these factors add up to an effective increase in the carrier density, which leads to the increasing $T_c$ in the N-rich zone. In the N-deficient zone, although the lattice parameter of GdN remains constant, the increasing N vacancies keep increasing the carrier density. As a result, $T_c$ continues to increase in the N-deficient zone, consistent with a carrier-mediated model of ferromagnetism in GdN.[13,15,19]

## V. SUMMARY

In summary, we have studied the correlation between the magnetic and the structural aspects of magnetron-sputtered GdN thin films, grown at ambient temperature. By varying the relative abundance of the component species during film growth, we varied the Gd-N ratio in the films and obtained samples in the N-rich and N-deficient regions of phase space. The saturation moment in the N-rich zone (zone 1 in Fig. 5) showed a low $M_s$, which increased with decreasing nitrogen fraction until it approached the theoretical value, symbolizing an optimum stoichiometry. Simultaneously, the Curie temperature approached the value of ~60 K. In the N-deficient zone (zone 2 in Fig. 5), the magnetic behavior and the structural properties changed considerably, in a coupled manner. While x-ray diffraction measurements showed the condensation of a secondary phase of GdN (GdN-II), in the N-deficient zone, the magnetization measurements showed enhanced $H_c$ and an exchange bias. The existence of the exchange bias confirmed an antiferromagnetic behavior of GdN-II (with a Nèel temperature of ~36 K[20]) and simultaneously explained the enhanced coercivity observed in the N-deficient region. A rough estimate of the volume fraction of the GdN and GdN-II phases (ratio of peak integral area from x-ray profile fitting) was consistent with the observed drop in $M_s$ and rise in $H_{Ex}$. The variation of $T_c$ with $N_2$ fraction is consistent with a carrier-mediated mechanism of ferromagnetism. We believe that N vacancies in our GdN films account for both the enhanced $T_c$ and antiferromagnetism. While electron doping of the conduction band by the N vacancy explains the enhanced $T_c$, the local lattice distortion caused by the vacancy is very likely to strengthen the antiferromagnetic superexchange over the nearest-neighbor ferromagnetic exchange, resulting in AFM behavior. Hall effect measurements showed that the carrier concentration in polycrystalline GdN films can be varied considerably by controlling the amount of nitrogen in the films, resulting in samples with widely varied transport properties, from almost-insulating to semimetallic behavior. Further experiments are needed to quantify the density of N vacancies and correlate it with the change in the lattice parameters and the enhanced $T_c$.

## ACKNOWLEDGMENTS

We thank Dr. A. Walton for the XPS measurements at the Leeds EPSRC Nanoscience and Nanotechnology Facility (LENNF). Financial support for this work was provided by the Leverhulme Trust.

*Corresponding author. kartikiitk@gmail.com

[1] J. J. Rhyne and T. R. McGuire, IEEE Trans. Magn. **8**, 105 (1972).
[2] E. Kaldis and C. Zurcher, Helv. Phys. Acta **47**, 421 (1974).
[3] R. A. Cutler and A. W. Lawson, J. Appl. Phys. **46**, 2739 (1975).
[4] A. Hasegawa and A. Yanase, J. Phys. Soc. Jpn. **42**, 492 (1977).
[5] P. Wachter, E. Kaldis, and R. Hauger, Phys. Rev. Lett. **40**, 1404 (1978).
[6] P. Wachter and E. Kaldis, Solid State Commun. **34**, 241 (1980).
[7] A. G. Petukhov, W. R. L. Lambrecht, and B. Segall, Phys. Rev. B **50**, 7800 (1994).
[8] J. Q. Xiao and C. L. Chien, Phys. Rev. Lett. **76**, 1727 (1996).
[9] T. Kasuya and D. X. Li, J. Magn. Magn. Mater. **167**, L1 (1997).
[10] D. X. Li, Y. Haga, H. Shida, T. Suzuki, Y. S. Kwon, and G. Kido, J. Phys. Condens. Matter **9**, 10777 (1997).
[11] F. Leuenberger, A. Parge, W. Felsch, K. Fauth, and M. Hessler, Phys. Rev. B **72**, 014427 (2005).
[12] P. Larson and Walter R. L. Lambrecht, J. Phys. Condens. Matter **18**, 11333 (2006).
[13] C. Duan, R. F. Sabiryanov, W. N. Mei, P. A. Dowben, S. S. Jaswal, and E. Y. Tsymbal, Appl. Phys. Lett. **88**, 182505 (2006).
[14] J. W. Gerlach, J. Mennig, and B. Rauschenbach, Appl. Phys. Lett. **90**, 061919 (2007).
[15] C. Duan, R. F. Sabirianov, W. N. Mei, P. A. Dowben, S. S. Jaswal, and E. Y. Tsymbal, J. Phys. Condens. Matter **19**, 315220 (2007).
[16] K. Doll, J. Phys. Condens. Matter **20**, 075214 (2008).
[17] C. Mitra and W. R. L. Lambrecht, Phys. Rev. B **78**, 134421 (2008).
[18] S. M. Ludbrook, I. L. Farrell, M. Kuebel, B. J. Ruck, A. R. H. Preston, H. J. Trodahl, L. Ranno, R. J. Reeves, and S. M. Durbin, J. Appl. Phys. **106**, 063910 (2009).
[19] A. Sharma and W. Nolting, Phys. Rev. B **81**, 125303 (2010).
[20] K. Senapati, T. Fix, M. E. Vickers, M. G. Blamire, and Z. H. Barber, J. Phys. Condens. Matter **22**, 302003 (2010).
[21] A. Schmehl, V. Vaithyanathan, A. Herrnberger, S. Thiel, C. Richter, M. Liberati, T. Heeg, M. Rockerath, L. Kourkoutis, S. Muhlbauer, P. Boni, D. A. Muller, Y. Barash, J. Schubert, Y. Idzerda, J. Mannhart, and D. G. Schlom, Nat. Mater. **6**, 882 (2007).
[22] S. Granville, B. J. Ruck, F. Budde, A. Koo, D. J. Pringle, F. Kuchler, A. R. H. Preston, D. H. Housden, N. Lund, A. Bittar, G. V. M. Williams, and H. J. Trodahl, Phys. Rev. B **73**, 235335 (2006).
[23] M. A. Ruderman and C. Kittel, Phys. Rev. **96**, 99 (1954); T. Kasuya, Prog. Theor. Phys. **16**, 45 (1956); K. Yosida, Phys. Rev. **106**, 893 (1957).
[24] D. D. Bacon, A. T. English, S. Nakahara, F. G. Peters, H. Schreiber, W. R. Sinclair, and R. B. van Dover, J. Appl. Phys. **54**, 6509 (1983).
[25] A. Barth, F. Treubel, M. Marszalek, W. Evenson, O. Hellwig, C. Borschel, M. Albrecht, and G. Schatz, J. Phys. Condens. Matter **20**, 395232 (2008).
[26] J. Nogués, D. Lederman, T. J. Moran, and I. K. Schuller, Phys. Rev. Lett. **76**, 4624 (1996).
[27] J. Sort, J. Nogués, S. Suriñach, J. S. Muñoz, M. D. Baró, E. Chappel, F. Dupont, and G. Chouteau, Appl. Phys. Lett. **79**, 1142 (2001).
[28] R. Coehoorn, D. B. de Mooij, and C. de Waard, J. Magn. Magn. Mater. **80**, 101 (1989).
[29] E. E. Fullerton, J. S. Jiang, and S. D. Bader, J. Magn. Magn. Mater. **200**, 392 (1999).
[30] M. D. Stiles and R. D. McMichael, Phys. Rev. B **63**, 064405 (2001).
[31] A. P. Malozemoff, Phys. Rev. B **35**, 3679 (1987).
[32] R. Kauffmann and O. Meyer, Solid State Commun. **51**, 539 (1984).
[33] A. Mauger and C. Godart, Phys. Rep. **141**, 51 (1986).
[34] C. Kittel, *Introduction to Solid State Physics*, 8th ed. (John Wiley, New York, 2005).
[35] M. I. Darby, Br. J. Appl. Phys. **18**, 1415 (1967).
[36] H. Ott, S. J. Heise, R. Sutarto, Z. Hu, C. F. Chang, H. H. Hsieh, H.-J. Lin, C. T. Chen, and L. H. Tjeng, Phys. Rev. B **73**, 094407 (2006).
[37] H. Miyazaki, H. J. Im, K. Terashima, S. Yagi, M. Kato, K. Soda, T. Ito, and S. Kimura, Appl. Phys. Lett. **96**, 232503 (2010).
[38] M. Barbagallo, N. D. M. Hine, J. F. K. Cooper, N.-J. Steinke, A. Ionescu, C. H. W. Barnes, C. J. Kinane, R. M. Dalgliesh, T. R. Charlton, and S. Langridge, Phys. Rev. B **81**, 235216 (2010).
[39] S. Demokritov, U. Rucker, and P. Grunberg, J. Magn. Magn. Mater. **163**, 21 (1996).
[40] Y. Shapira, S. Foner, and T. B. Reed, Phys. Rev. B **8**, 2299 (1973).